nature communications

Article

https://doi.org/10.1038/s41467-023-41681-0

Towards bioresource-based aggregation-induced emission luminogens from lignin β-O-4 motifs as renewable resources

Received: 26 April 2023

Accepted: 14 September 2023

Published online: 28 September 2023

Check for updates

Tenglong Guo[1,5], Yuting Lin[2,5], Deng Pan[3,5], Xuedan Zhang[2], Wenqing Zhu[1], Xu-Min Cai[2] ✉, Genping Huang[3] ✉, Hua Wang[1], Dezhu Xu[1], Fritz E. Kühn[4], Bo Zhang[1] ✉ & Tao Zhang[1] ✉

One-pot synthesis of heterocyclic aromatics with good optical properties from phenolic β-O-4 lignin segments is of high importance to meet high value added biorefinery demands. However, executing this process remains a huge challenge due to the incompatible reaction conditions of the depolymerization of lignin β-O-4 segments containing γ-OH functionalities and bioresource-based aggregation-induced emission luminogens (BioAIEgens) formation with the desired properties. In this work, benzannulation reactions starting from lignin β-O-4 moieties with 3-alkenylated indoles catalyzed by vanadium-based complexes have been successfully developed, affording a wide range of functionalized carbazoles with up to 92% yield. Experiments and density functional theory calculations suggest that the reaction pathway involves the selective cleavage of double C-O bonds/Diels-Alder cycloaddition/dehydrogenative aromatization. Photophysical investigations show that these carbazole products represent a class of BioAIEgens with twisted intramolecular charge transfer. Distinctions of emission behavior were revealed based on unique acceptor-donor-acceptor-type molecular conformations as well as molecular packings. This work features lignin β-O-4 motifs with γ-OH functionalities as renewable substrates, without the need to apply external oxidant/reductant systems. Here, we show a concise and sustainable route to functional carbazoles with AIE properties, building a bridge between lignin and BioAIE materials.

Both the damaging environmental impact and the increasing depletion of fossil resources have triggered strong interest in utilizing biomass for helping to satisfy the growing energy demand in a sustainable form as well as a source for basic chemicals[1,2]. As a high volume and fairly cheap renewable resource, lignin is a unique precursor for the production of aromatic chemicals[3,4]. With respect to structural moieties, β-O-4 (β-aryl ether) associated with γ-OH is the most abundant linkage in lignin, making up approximately 50–65% of all linkages, dependent

[1]CAS Key Laboratory of Science and Technology on Applied Catalysis, Dalian Institute of Chemical Physics, Chinese Academy of Sciences, Dalian 116023, China. [2]Jiangsu Co-Innovation Center of Efficient Processing and Utilization of Forest Resources, International Innovation Center for Forest Chemicals and Materials, College of Chemical Engineering, Nanjing Forestry University, Nanjing 210037, China. [3]Department of Chemistry, School of Science and Tianjin Key Laboratory of Molecular Optoelectronic Sciences, Tianjin University, Tianjin 300072, China. [4]Molecular Catalysis, Catalysis Research Center and Department of Chemistry, Technical University of Munich, Lichtenbergstr. 4, D-85748 Garching bei München, Germany. [5]These authors contributed equally: Tenglong Guo, Yuting Lin, Deng Pan. ✉e-mail: xumin.cai@njfu.edu.cn; gphuang@tju.edu.cn; bo.zhang@dicp.ac.cn; taozhang@dicp.ac.cn

https://doi.org/10.1038/s41467-023-41681-0

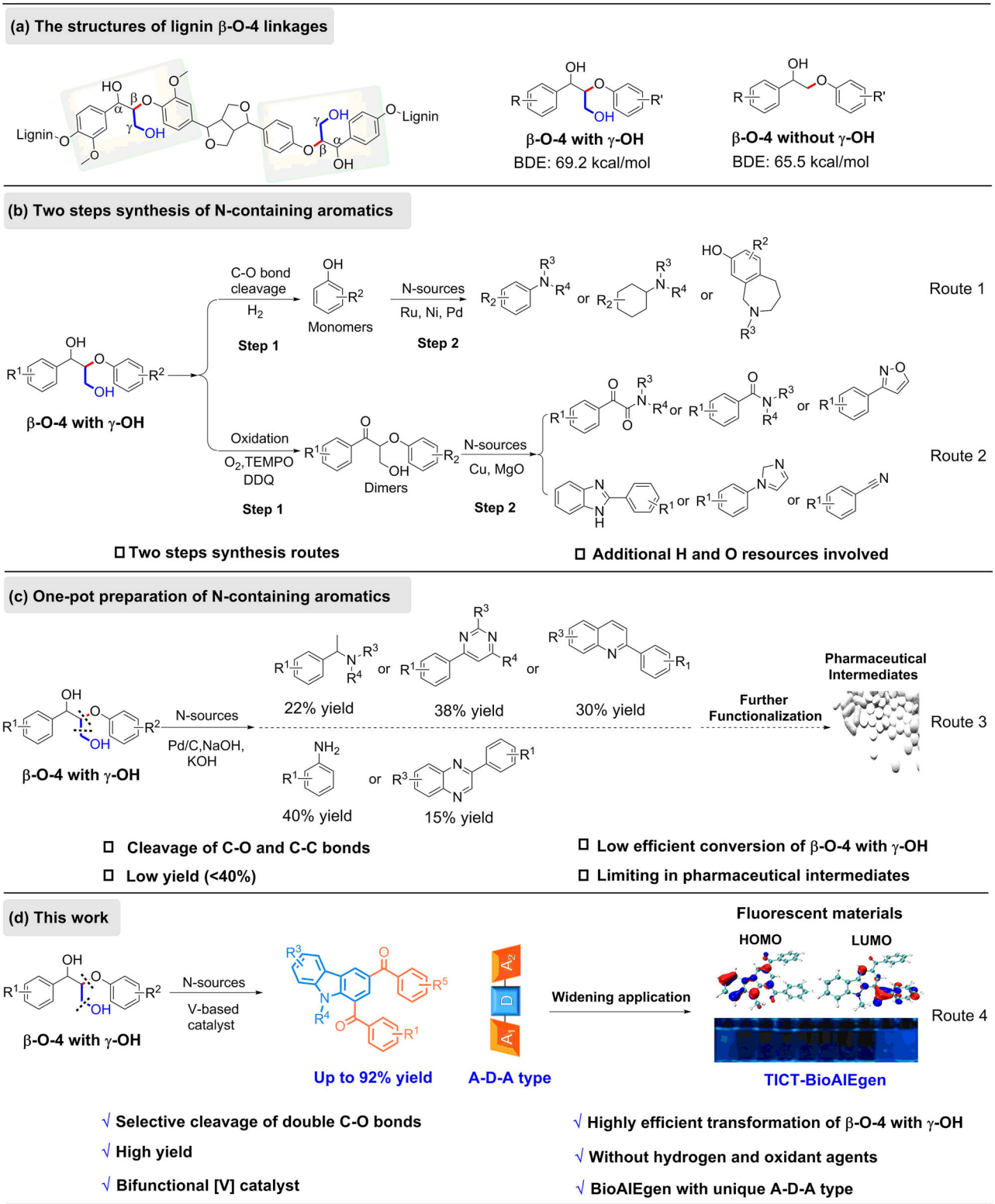

Fig. 1 | N-participated depolymerization of lignin phenolic β-O-4 motifs containing γ-OH groups. a Structures of lignin β-O-4 motifs; **b** synthesis of N-containing aromatics from lignin β-O-4 with γ-OH through two steps; **c** one-pot synthesis of N-containing aromatics from lignin β-O-4 with γ-OH; **d** construction of carbazole-based BioAIEgen from lignin β-O-4 with γ-OH.

on the lignin type (Fig. 1a)[5]. Effective depolymerization of this particular linkage could not only remove a considerable barrier in the degradation of lignin feedstocks, but also provide useful depolymerized molecules as scaffolds for potential applications. Thus, extensive efforts have been dedicated to deconstruct the β-O-4 motif to deliver C, H, O-containing products with additional hydrogen and oxygen donating agents. With the aim to functionalize lignin downstream products further, introduction of nitrogen to form nitrogen-containing aromatics is also emerging and increasingly brought into focus[6–8]. So far, most of the current strategies are limited to the

employment of lignin-derived monophenols or modified β-O-4 dimers as starting materials to produce N-containing aromatics in the presence of a N-source through one or multiple steps[9–19] (Fig. 1b, Routes 1–2). Additionally, hydrogenation and oxidation processes are unavoidable. As a challenge, the direct transformation of phenolic β-O-4 linkages to N-containing aromatics without external H or O source is still prominent. Building on recent progress, our group and that of Jiao independently developed methods for the preparation of various N-containing aromatics (benzylamines, pyrimidines, quinolines, quinoxalines and anilines) with organic amines or NaN_3 as N-sources through controlled cleavage of the C-O bond in β-O-4 motifs and the construction of C-C/C-N bonds in a one-pot fashion (Fig. 1c, Route 3)[20–24]. However, these systems exhibit low efficiency and poor selectivity when meeting β-O-4 moieties containing γ-OH groups, leading to low yields of N-containing aromatics (<40%). The higher bond dissociation energies of β-O-4 linkage with γ-OH (69.2 kcal/mol)[25] compared with β-O-4 without γ-OH (65.5 kcal/mol)[26] leads to a variety of unwanted by-products, which is the main reason of lower yield. Moreover, the target molecule application is so far largely confined to the synthesis of medicinal intermediates, large volume application is prohibited by the need of further functionalization. Therefore, the development of a simple and efficient strategy for the production of N-containing aromatics would lead to new applications of lignin-based chemicals.

Bio-resource derived aggregation-induced emission luminogens (BioAIEgens, AIEgens or AIE-active nano agents obtained from natural resources including natural products or derivatives by modifying natural products)[27–30] have raised considerable attention owing to their advantageous renewability, biodegradability, and biocompatibility, paving the way to potential applications in biomedical[31–33], chemosensors/biosensors[34,35], and optoelectronic devices[36,37]. As a natural biomass rich in aromatic and carbonyl subunits, lignin based building blocks display strong fluorescence and excellent self-assembly properties, which could make them serve as ideal precursors for the preparation of BioAIEgens[33,38–40]. However, its complex structure makes it difficult to controllably degrade, thereby limiting the application of lignin. Current studies are usually limited to macromolecular BioAIEgens directly coming from lignin itself or structurally modified lignin based macromolecules, resulting in the fact that the luminescence mechanism and structure-property relationships are still unclear due to the complicated and uncontrollable macromolecular structures. Therefore, the efficient and controllable conversion of lignin platform chemicals into value-added fine chemicals has become a hot research topic for utilization of lignin. Therefore, obtaining BioAIEgens with well-defined structures through lignin depolymerization would provide an alternative strategy for the design of lignin-derived BioAIEgens. Conventional state of the art design of AIEgens is based on restriction of intramolecular motion[41]. Moreover, the construction of electronic donor-acceptor (D-A) configuration is regarded as an effective approach to manipulate the properties of luminescent materials[42,43]. One type of D-A structured molecules, namely the D-A-D type, has attracted considerable interest[44–46]. In contrast, reports on A-D-A molecules as luminescent materials are relatively limited. In recent years, some reports suggest that A-D-A compounds can exhibit stronger charge transfer effects and light-harvesting capability compared to D-A-D structure, hence holding great potential in organic photovoltaics and biomedical applications[47–50]. BioAIEgen associated with A-D-A configuration may synchronously regulate the photophysical properties. Hence, developing a concise and sustainable route to construct BioAIEgens with A-D-A configuration would be a great achievement and highly desirable as potential phototheranostic agents.

Carbazole is an important N-containing heterocyclic organic compound with low ionization potential and a strong electron donor ability[51], these features make them as an ideal electron donor to construct D-A structures[52–55]. Employing carbazole as a core moiety, introducing two electron acceptor groups (i.e., benzoyl) into a carbazole scaffold might provide an efficient way for the preparation of A-D-A-type AIEgens. Moreover, extensive synthetic strategies of the functionalized carbazoles focus on intermolecular cross-coupling reactions between C-H/C-X bonds (X = halo, N, O, C, etc)[56], oxidative intramolecular C-H/C-H cross coupling of prefunctionalized diarylamines[57], the construction of a benzene ring upon substituted indoles through transition metal catalysis[58] or Brønsted acid catalysis[59–61]. However, most approaches suffer from the need of excess oxidants, multi-step reactions and the formation of non-renewable substrates, which raises atom economy and environmental concerns. Thus, a sustainable protocol for producing carbazoles synthesis is desirable.

In this work, we developed a sustainable route for the production of functionalized carbazoles through transformation of lignin β-O-4 segments. γ-OH groups of β-O-4 could be well tolerated. Furthermore, the establishment of the triangular A-D-A skeleton, based on the electron donor ability of carbazole and the corresponding electron acceptor behavior of benzoyl resulting from this unique synthetic methodology has successfully led to the desired twisted intramolecular charge transfer (TICT) AIE properties (Fig. 1d, Route 4).

Results and discussion

Reaction optimization

Initially, β-O-4 linkages containing a γ-OH group (**1a**), highly abundant in natural lignin, are selected as a probe reaction with alkenylated indole **2a** catalyzed by vanadium associated with tridentate Schiff base ligands (V-based complexes)[62]. The results show that carbazole derivative **3a** as a target product forms in 89% yield along with guaiacol (**4a**) in 99% yield (Supplementary Table 1, entry 1), demonstrating that carbazole formation occurs, associated with a selective C-O bond cleavage of the lignin model compound, C-C bond construction and dehydrogenation/aromatization in a one-pot fashion. Based on this exciting reactivity, the experiment parameters (catalyst loading, substrates ratio, and reaction temperature) are optimized (Supplementary Tables 1–3). Screening various solvents reveal that the reaction proceeds most efficiently in toluene, compared to N, N-dimethylformamide (DMF), CH_3OH, CH_3CN, tetrahydrofuran and H_2O (Supplementary Table 1, entries 1–6). Additionally, the reaction is very sensitive to reaction temperature. Upon lowering the temperature, yield of **3a** decreases significantly from 89% at 140 °C to 76% at 120 °C (Supplementary Table 1, entries 1, 7–8). In contrast, changing the catalyst to commercial $VO(OEt)_3$ and 2,2′-bipyridine ligand, the carbazole **3a** is formed only in 55% yield (Supplementary Table 1, entry 9). Notable, a blank experiment shows that without catalyst no product is formed (Supplementary Table 1, entry 10), illustrating the V-based catalyst indeed plays a crucial role.

Substrate scope

A broad spectrum of substrates with varying electronic and steric effects, and various functional groups on the aromatic ring of the lignin model compound **1** and alkenylated indoles **2** in the presence of V-based catalyst is explored, affording good to excellent yields of the corresponding carbazole derivatives **3**. As shown in Fig. 2, lignin β-O-4 model substrates **1a** and **1b** bearing methoxy substituents on the aryl moieties associated with **2a** as a reaction partner to generate the target carbazole products **3a** and **3b** lead to 91% and 86% isolated yield, along with 99% and 85% yield of guaiacol **4a**, respectively (Fig. 2, entries 1–2). To our delight, the reaction also tolerates a hydroxyl group on the aryl ring of **1c**, yielding 71% of **3c** (Fig. 2, entry 3). Compound **1d** bearing no functional group leads to a somewhat reduced yield of carbazole **3d** (61%) and of phenol **4b** (76%) (Fig. 2, entry 4), illustrating that methoxyl groups on the aryl ring of **1** execute a positive influence on the reaction efficiency. It is noteworthy that N-induced deconstruction of lignin β-

https://doi.org/10.1038/s41467-023-41681-0

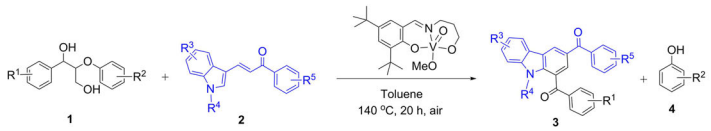

Entry	Substrate 1	Substrate 2	Products	
			3 Yield[a]	4 Yield[b]
1	1a	2a	3a, 91%(89%)[b]	4a, 99%
2	1b	2a	3b, 86%	4a, 85%[a]
3	1c	2a	3c, 71%	4a, 81%[a]
4	1d	2a	3d, 61%	4b, 76%[a]
5	1a	2b	3e, 86%	4a, 96%
6	1a	2c	3f, 80%	4a, 84%
7	1a	2d	3g, 91%	4a, 90%
8	1a	2e	3h, 92%	4a, 80%
9	1a	2f	3i, 75%	4a, 85%
10	1a	2g	3j, 53%	4a, 99%
11	1a	2h	3k, 83%	4a, 80%
12	1a	2i	3l, 84%	4a, 91%
13	1a	2j	3m, 85%	4a, 91%
14	1a	2k	3n, 81%	4a, 92%
15	1a	2l	3o, 72%	4a, 99%
16	1a	2m	3p, 63%	4a, 97%
17	1a	2n	3q, 84%	4a, 95%
18	1a	2o	3r, 84%	4a, 79%
19	1a	2p	3s, 65%	4a, 82%
20	1a	2q	3t, 95%	4a, 97%
21	1a	2r	3u, 87%	4a, 86%
22	1a	2s	3v, 68%	4a, 84%

Fig. 2 | Synthesis of carbazole derivatives 3 with various substrates 1 and 2. Reaction conditions: **1** (0.4 mmol), **2** (0.2 mmol), V-complex catalyst (10 mol%), toluene (4 mL) in air, 140 °C, reaction time (t) = 20 h, yields of **3** and **4** are calculated based on the amounts of **2** and **1**, respectively. [a]Isolated molar yield. [b]Yields are determined by HPLC with an external standard method.

O-4 linkages containing γ-OH group generally produces lower yields (<40%) of N-containing aromatics due to the complicated structure and higher steric hindrance[20–24]. With the catalytic system applied here, β-O-4 motifs with γ-OH **1a**–**1d** are efficiently transformed to carbazole derivatives **3a**–**3d** in high isolated yields (61–91%). In contrast, the reaction of a N-H free indole derivative ((*E*)-3-(1*H*-indol-3-yl)-1-phenylprop-2-en-1-one) with **1d** is carried out, leading to ((*E*)-3-(1-(3-oxo-3-phenylpropyl)-1*H*-indol-3-yl)-1-phenylprop-2- en-1-one as main product

https://doi.org/10.1038/s41467-023-41681-0

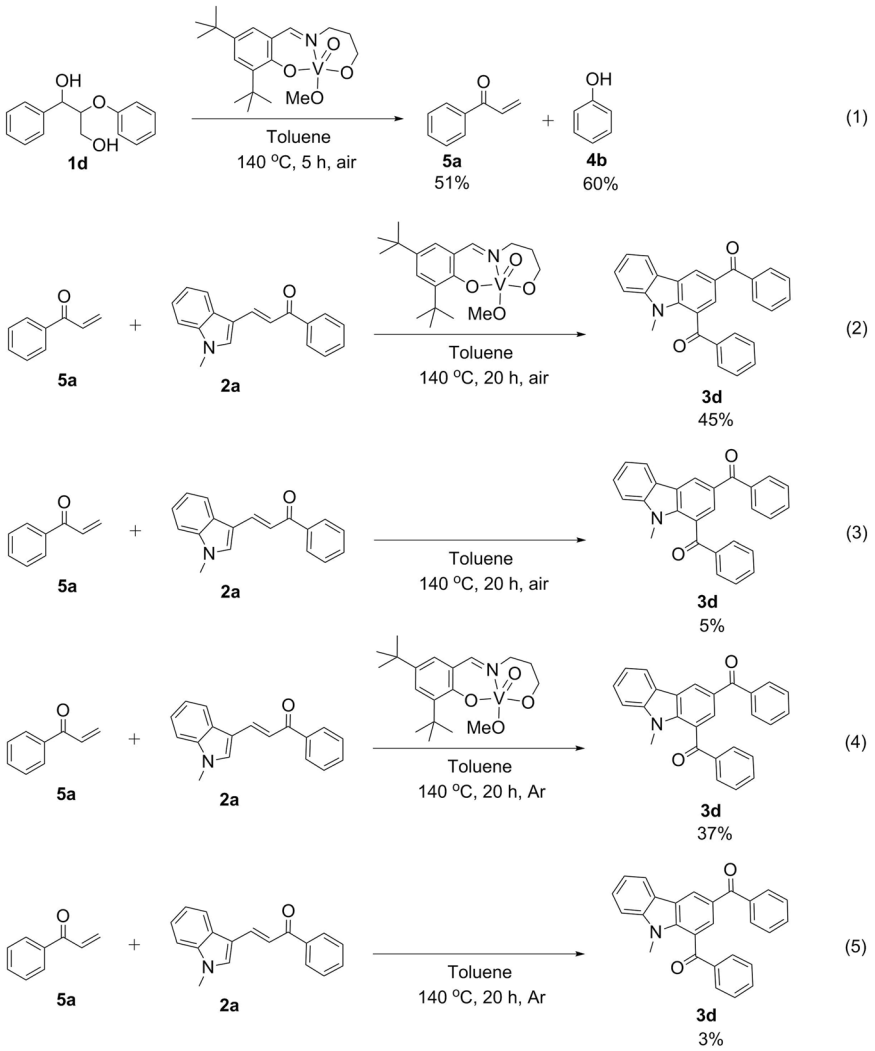

Fig. 3 | Mechanistic experiments. (1) selective C-O bond cleavage of **1d** catalyzed by V-complex catalyst; (2)–(3) the reactions with and without V-complex catalyst under air; (4)–(5) the reactions with and without V-complex catalyst under argon environment.

in 21% yield due to some side reactions (Supplementary Fig. 1). In order to obtain high selectivity of carbazole products, N-protected indole derivatives (**2a**–**2s**) are used as substrates. For example, a benzyl substituent on the N-R moiety in 3-alkenylated is tolerated, leading to 86% yield of **3e** (Fig. 2, entry 5). Additionally, electron-donating substituents such as –Me and -OCH_3 on the aryl rings of the indole moieties apparently do not affect the reaction efficiency, since **3f**–**3h** are obtained in 80–92% yield (Fig. 2, entries 6–8), whereas an electron-withdrawing Cl- group decreases the yield of product **3i** to 75% (Fig. 2, entry 9). To further investigate the scope of this reaction, various substituents on the phenyl moiety of the alkenylated indoles **2** were applied. The substrates bearing-Me groups in meta- or para- position lead to **3k** and **3l** (83% and 84%) in higher yields compared with a Me group in ortho-position (**3j**, 53%) due to the steric hindrance in the latter case (Fig. 2, entries 10–12). No obvious electronic effect was detected for the substituted group on the aryl moiety of **2** in this transformation. *P*-Me, *p*-OCH_3, *p*-F, *p*-Cl, *p*-CN and aryl substituted alkenylated indoles **2** proceed to deliver the expected products **3l**–**3r** in 63–85% yield (Fig. 2, entries 11–18). Moreover, a tribenzene-alkene bearing substrate also react smoothly, giving the target product **3s** in moderate yield (65%) (Fig. 2, entry 19). Notably, heterocyclic functionalities such as thiophene and furan groups also allow the formation of carbazole derivatives **3t** and **3u** in 95% and 87% yield (Fig. 2, entries 20–21). Beyond that, this process is also effective for a substrate containing an alkyl ring, obtaining target product **3v** in 68% yield (Fig. 2, entry 22). Significantly, the phenol products **4a**–**4b**, being valuable precursors of detergents, pesticides, antimicrobials and pharmaceutical drugs[63], can be obtained in yields of 76–99%. All these results demonstrate that the system described in this work displays excellent tolerance to a broad substrate scope, not only providing access to carbazole derivatives in high isolated yields, but also achieving phenol derivatives in excellent yields, greatly increasing atom-economy.

Mechanistic studies

With the aim to elucidate the mechanism of this cascade reaction, several control experiments are carried out. The initial and crucial step is the selective cleavage of double C-O bonds of the lignin β-O-4 with γ-OH motif with the assistance of the V- catalyst, determining the downstream reaction. Thus treatment of **1d** alone under standard conditions yields 51% of enone (**5a**) and 60% of **4b** (Equation 1, Fig. 3). Then the reaction of **5a** with **2a** affords the desired product **3d** in 45% yield (Equation 2, Fig. 3), indicating that **5a** is a key intermediate. Compared to 61% yield of **3d** in Entry 4 Fig. 2 using **1d** as a starting material, this lower yield is due to **5a** being very unstable and an easily occurring side reactions at the rather high temperature of 140 °C[64], in situ generated enone **5a** from the lignin β-O-4 segment is more efficiently converted to carbazole. Aiming to verify the dehydrogenation

https://doi.org/10.1038/s41467-023-41681-0

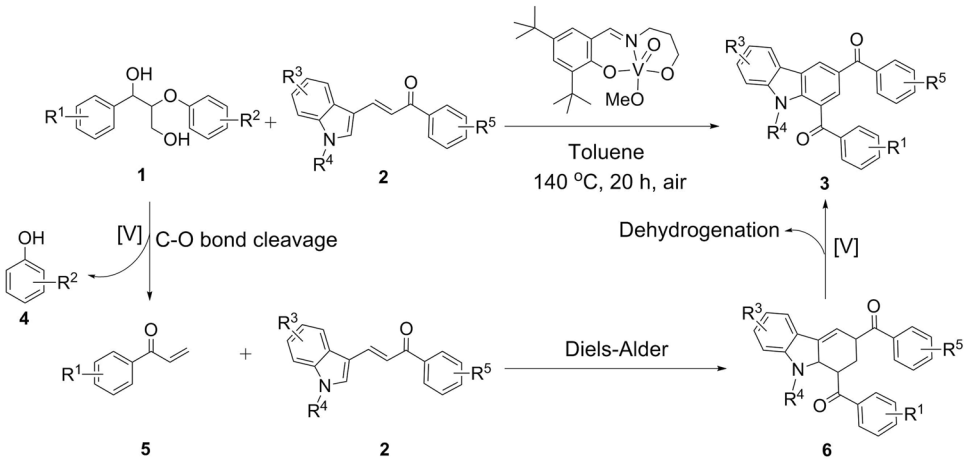

Fig. 4 | Proposed pathway. Proposed pathway for the production of carbazoles from lignin β-O-4 motifs ([V] refers to V-complex catalyst).

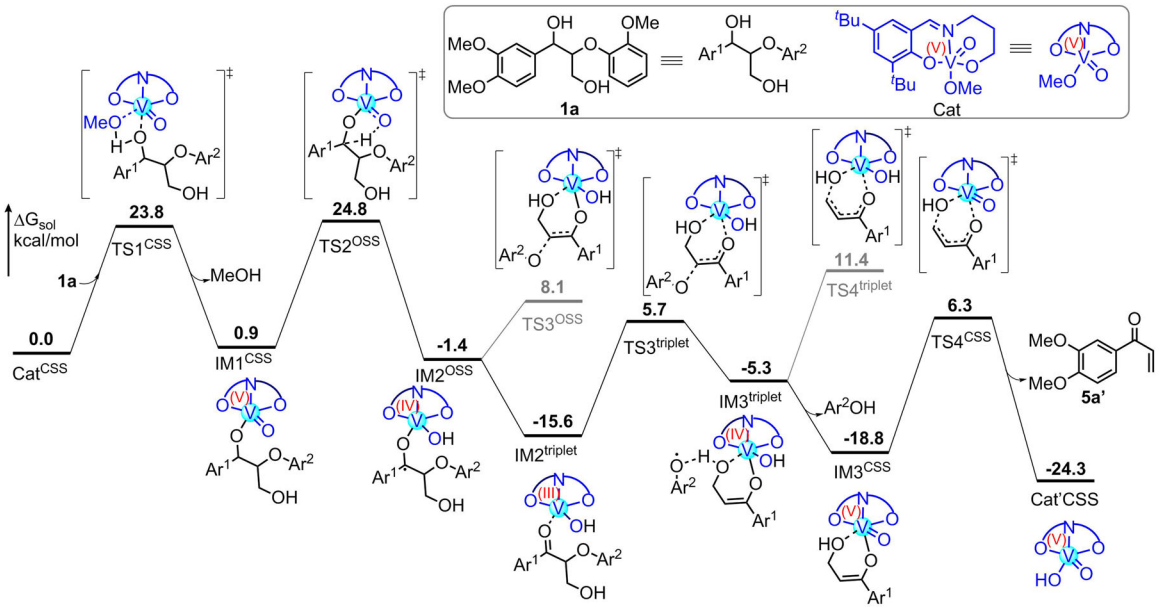

Fig. 5 | Computational analysis. Calculated energy profile of the V-complex catalyzed selective C-O bond cleavage of **1a** (CSS refers to closed-shell singlet and OSS refers to open-shell singlet).

ability of the V-catalyst, the same reaction as given in Equation 2 is performed in the absence of catalyst (Equation 3, Fig. 3). However, only 5% yield of **3d** are obtained (Equation 3, Fig. 3). Similarly, the reactions of **5a** with **2a** with and without V-catalyst are also conducted under argon atmosphere (Equations 4 and 5, Fig. 3), showing that the target product **3d** is formed in 37% yield with V-catalyst, compared with 3% yield of **3d** in the absence of V-catalyst. These results show that the V-catalyst plays an important role for the subsequent intramolecular dehydrogenation. On the basis of these results, a plausible reaction pathway is proposed in Fig. 4: lignin β-O-4 model compounds initially undergo selective V-catalyzed cleavage of the C-O bond to release enones **5** and phenol co-products **4**. Then **5** reacts with **2** via a Diels-Alder cycloaddition to form tetrahydrocarbazoles backbone **6**, which subsequently generates the final product **3** through dehydroaromatization. In the whole reaction the V-complex acts as a bifunctional catalyst for both the selective cleavage of the C-O bond of the lignin β-O-4 model compounds and for the dehydrogenation process.

To gain deeper insight into the detailed reaction mechanism of the vanadium-complex catalyzed selective C-O bond cleavage, density functional theory (DFT) calculations are performed. The calculated energy profile of the vanadium-catalyzed selective C-O bond cleavage of **1a** is given in Fig. 5 and Supplementary Table 4 as well as Supplementary Data 1.

The reaction is proposed to be initiated by a ligand exchange between the V-catalyst Cat^{CSS} and the benzylic hydroxyl group of **1a** to give intermediate $IM1^{CSS}$ and MeOH, which is agreement with previous work[62]. This process is found to occur via a four-membered transition state $TS1^{CSS}$, with an energy barrier of 23.8 kcal/mol. Then, intermediate $IM1^{CSS}$ undergoes an intramolecular hydrogen transfer via transition state $TS2^{OSS}$ with an energy barrier of 23.9 kcal/mol relative to $IM1^{CSS}$, leading to intermediate $IM2^{OSS}$. The calculations show that the ensuing C(sp^3)-O bond cleavage directly from intermediate $IM2^{OSS}$ takes place via transition state $TS3^{OSS}$, which is 9.5 kcal/mol higher in energy than $IM2^{OSS}$. Alternatively, it is found that a spin-crossover phenomenon from a singlet spin state to a triplet spin state can occur to yield the very stable ketone-coordinated V(III) $IM2^{triplet}$, from which the C(sp^3)-O bond cleavage via transition state $TS3^{triplet}$ is slightly more favored with an energy barrier of 21.3 kcal/mol relative to $IM2^{triplet}$.

https://doi.org/10.1038/s41467-023-41681-0

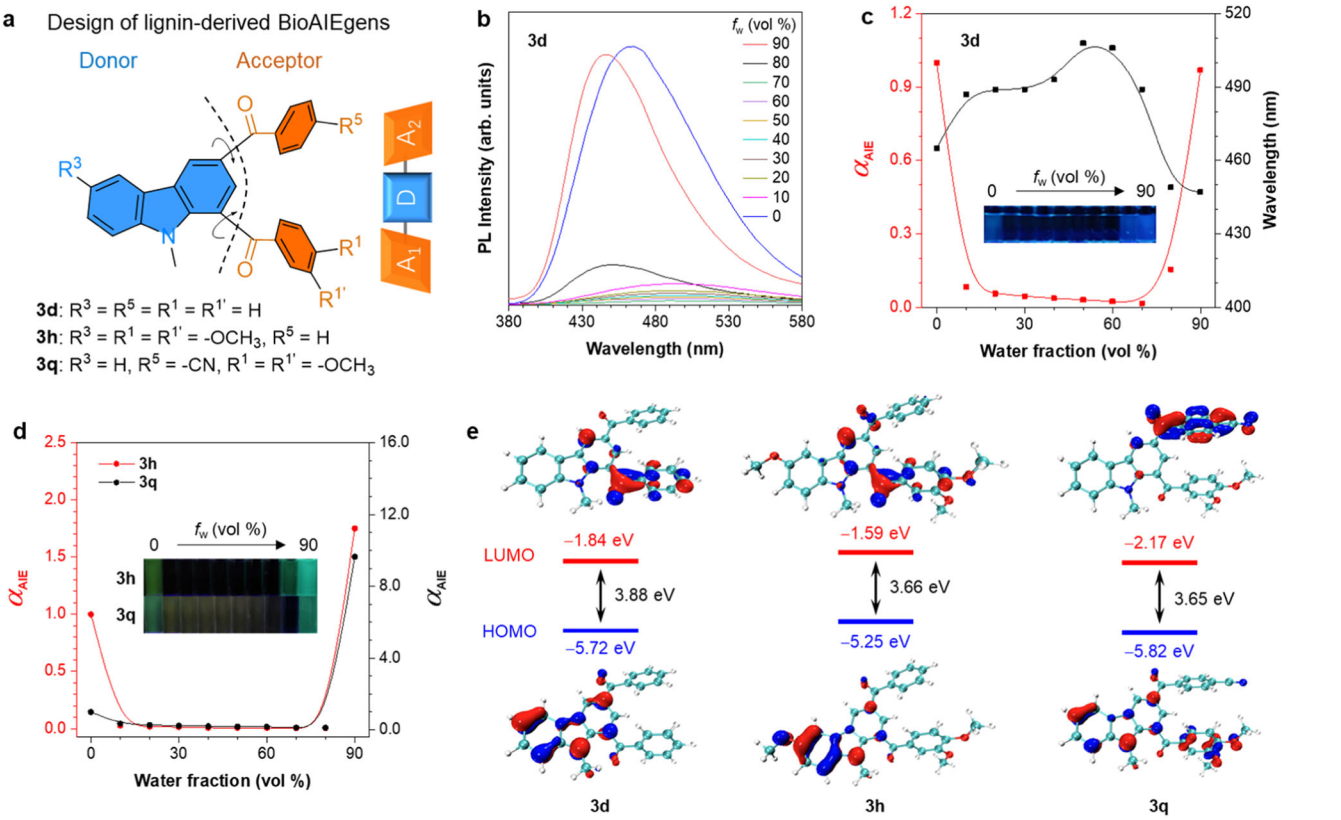

Fig. 6 | Investigation of optical properties. a Molecular design of lignin-derived BioAIEgens; **b** PL spectra of **3d** in acetonitrile/water (ACN/H_2O) mixtures with different water fractions (f_w), λ_{ex}: 300 nm, concentration: 20 μM; **c** the plots of the α_{AIE} and maximum emission wavelength versus the composition of the aqueous mixture of **3d,** $\alpha_{AIE} = I/I_0$, I_0 = PL intensity in pure ACN, inset: fluorescence photographs taken under 365 nm UV irradiation; **d** plots of α_{AIE} versus the composition of the aqueous mixture of **3h** (I_0 = PL intensity in pure ACN, λ_{ex}: 311 nm) and **3q** (I_0 = PL intensity in pure THF, λ_{ex}: 301 nm), inset: fluorescence photographs taken under 365 nm UV irradiation, concentration: 20 μM; **e** frontier molecular orbitals and their corresponding HOMO/LUMO energies of **3d, 3h**, and **3q**.

Finally, the reaction is completed by a hydroxyl group elimination to deliver enone product **5a′**. The results show that hydroxyl group elimination via a triplet spin state transition state $TS4^{triplet}$ is much higher in energy than that via singlet spin state transition state $TS4^{CSS}$ (11.4 versus 6.3 kcal/mol), showing that the spin-crossover phenomena from triplet spin state ($IM3^{triplet}$) to singlet spin state ($IM3^{CSS}$) has to occur prior to the hydroxyl group elimination. Taken all results together, the hydroxyl group elimination is found to be the rate-determining step of the overall catalytic cycle, with an energy barrier of 25.1 kcal/mol.

Investigation of optical properties

Additional to establishing a sustainable synthesis of carbazole derivatives their optical properties have been studied as well. It is interesting to note that the carbazole backbones of **3a**–**3v** do possess a chemical structure of two benzoyl moieties as electronic acceptors on the meta positions of the electronic donor of carbazole, constituting a triangular A_1-D-A_2 configuration (Fig. 6a). The substrates involved herein have four changeable substituents on the A_1-D-A_2 skeleton, endowing most of them with AIE properties and distinct emission behavior (Supplementary Figs. 36–57). Represented by the non-substituted A-D-A skeleton of **3d** (Fig. 6b, c), the PL intensity decreases immediately when water is added, accompanied by a red-shifted emission that is also observed in a solvent effect experiment with increased solvent polarity (Supplementary Fig. 58), indicating the existence of TICT property[65,66]. When f_w increases up to 80%, the fluorescence revives, which is a typical feature of an AIE property. This might be because the restriction of intramolecular motion in the nanoaggregates leads to an intensified emission (Supplementary Fig. 59). For **3h** and **3q**, the photophysical properties in the aqueous mixtures show a similar trend as that of **3d**, implying that they have TICT-AIE properties as well (Fig. 6d, Supplementary Figs. 43 and 52). In order to shed more light on these observations, DFT calculations were carried out (Fig. 6e), showing CT effects with an electron shift to the LUMO, which is located either on A_1 or on A_2, dependent on the substituents. **3d** displays electrons localized on carbazole in the HOMO and an A_1 localized LUMO, respectively. Location of the LUMO on A_1 may be due to its unsymmetrical A_1-D-A_2 motif. For **3h**, the substitution of two electron-donating methoxy groups on both D and A_1 weakens the electron-acceptor ability of A_1, with the LUMO not only localized on A_1 but also slightly extending to A_2. With regard to **3q**, the LUMO mainly concentrates on A_2, owing to the strong electron withdrawing ability of the −CN group. The variable substitutions not only cause varied electronic distributions and locations of HOMO and LUMO, but also lead to different energy differences (band gaps) between the frontier orbitals as exemplified for **3d** (3.88 eV), **3h** (3.66 eV), and **3q** (3.65 eV), matching well with their luminescence colors. These results imply that the electronic distributions can be adjusted by altering the substituents on the A_1-D-A_2 skeleton, which can help to regulate the photophysical properties of the respective lignin-derived BioAIEgens.

In addition to the fluorescence behavior in solution and aggregate states, the photophysical properties in the solid state have been further studied. With the aim of investigating the structure-property relationships of solid-state fluorescence materials, single crystals of **3p** and **3q** have been obtained for further analysis. Similar to the solution and aggregate states, the unsubstituted solid state of **3d** still exhibits blue-violet fluorescence with a wavelength of 436 nm. **3p** and **3q** show a significant red-shift (**3p**: 493 nm; **3q**: 511 nm) compared to **3d**, probably

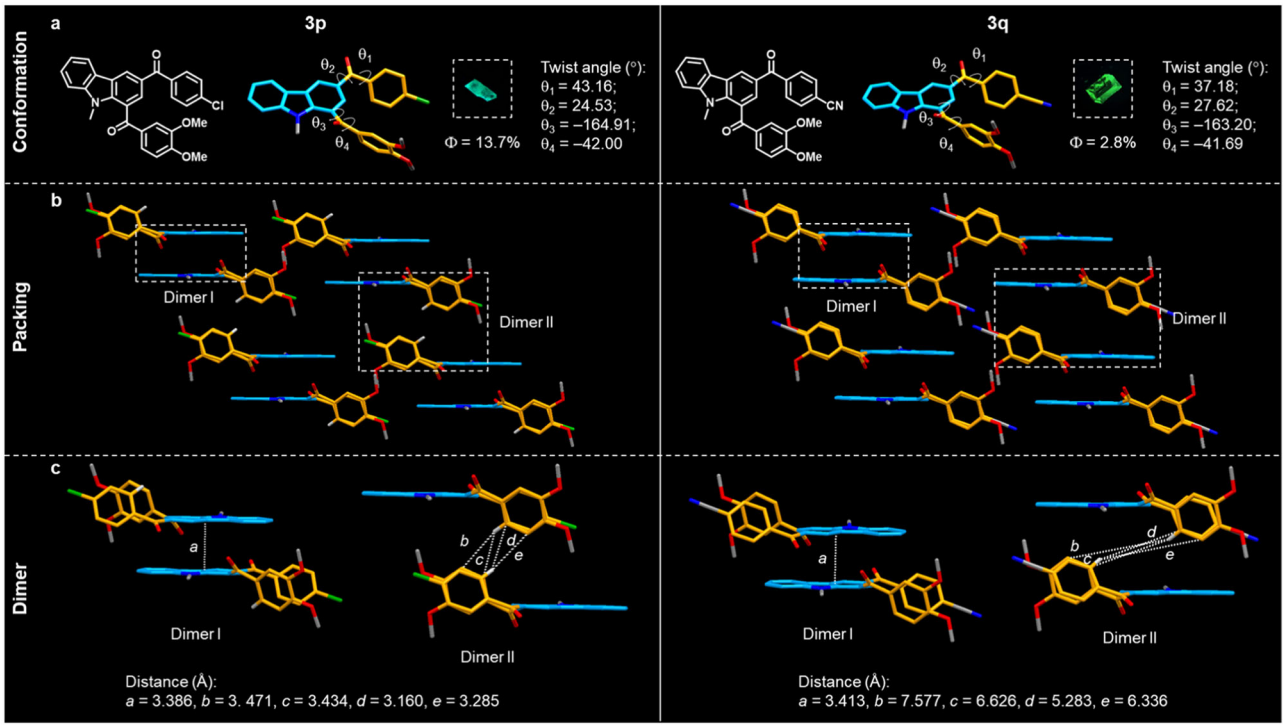

Fig. 7 | The crystal structures of 3p **and** 3q**. a** Molecular conformation of **3p** and **3q**; **b** packing of **3p** and **3q**; **c** respective dimer structures of **3p** and **3q**.

due to the presence of electronically different substituents[67,68], thus enhancing the characteristics of CT effects. With regard to the emission intensity, the solid-state quantum yield values of **3d, 3p**, and **3q** are 3.5%, 13.7% and 2.8%, respectively, and these trends are identical to the emission intensity reported in the solid-state emission spectra (Supplementary Fig. 60). In order to uncover the causes for the differences in emission intensity, the crystal structures of **3p** and **3q** have been analyzed in detail (Fig. 7 and Supplementary Table 5). The results show that the torsion angles at four comparable positions of **3p** (43.16°, 24.53°, −164.91°, −42.00°) and **3q** (37.18°, 27.62°, −163.20°, −41.69°) are quite close to each other, indicating similar molecular conformations (Fig. 7a). In addition, the packing modes of **3p** and **3q** are similar as well, giving two types of dimer modes (dimers I and II) (Fig. 7b). Further analysis demonstrates that they display slight differences in the fundamental structures of the two types of dimers (Fig. 7c). Specifically, in dimer I, the interplanar distances between the carbazole planes of **3p** (3.386 Å) and **3q** (3.413 Å) are quite similar. However, in dimer II, the four benzene rings between the two molecules constituting the dimer II in **3p** exhibit intermolecular C···H distances from 3.160 to 3.471 Å. The distances between the four benzene rings in **3q** are quite long (5.283–7.577 Å), exceeding the normal intermolecular interactions, giving rise to the weaker solid-state emission of **3q**[69,70]. The above described results suggest that in the case of very similar conformations subtle differences between dimers in the packing structures can nevertheless play a prominent role for the observed emission intensities.

In summary, a vanadium-catalyzed direct transformation of phenolic β-O-4 lignin segments, containing γ-OH with 3-alkenylated indoles has been developed for the construction of carbazole-based bioAIEgens without an external H/O resource. A selective tandem cleavage of two C-O bonds /Diels–Alder cycloaddition/dehydrogenative aromatization sequence is established as the reaction pathway, both through experimental studies and DFT calculations. As intended, the lignin-derived carbazoles with A-D-A configurations exhibit TICT-AIE performance, endowing the lignin-depolymerized derivatives with unique photophysical properties. The present protocol provides a concise and sustainable route to functionalized carbazoles with AIE properties from renewable substrates, creating a bridge between lignin and BioAIEgens.

Methods

Typical procedure for carbazole derivatives synthesis from lignin β-O-4 model compounds

Quantification of phenol derivatives: lignin model compound **1** (0.4 mmol), alkenylated indole **2** (0.2 mmol), catalyst (10 mol%) and toluene (4 mL) are added into a pressure tube (35 mL). The mixture was sealed and heated to 140 °C for 20 h. After reaction, the solution is cooled to room temperature, and diluted to 25 mL volumetric flask with DMF. The phenol derivatives are analyzed by HPLC using an external standard calibration curve method. Quantification of carbazole derivatives: lignin model compound **1** (0.4 mmol), alkenylated indole **2** (0.2 mmol), catalyst (10 mol%) and toluene (4 mL) are added into a pressure tube (35 mL). The mixture is sealed and heated to 140 °C for 20 h. After reaction, the solution is cooled to room temperature. The carbazole products are purified by column chromatography using petroleum ether/ethyl acetate (3:1) to give the isolated yield.

Computational details

All the calculations are performed at the (u)B3LYP-D3(BJ)[71–73] level of theory using Gaussian 09 package[74]. The geometry optimizations are carried out with a mixed basis set of LANL2TZ(f) for V and 6–31 G(d,p) for other atoms. Frequencies are computed analytically at the same level of theory to confirm whether the structures are minima (no imaginary frequencies) or transition states (only one imaginary frequency). Selected transition-state structures are confirmed to connect the correct reactants and products by intrinsic reaction coordinate calculations[75,76]. To obtain better accuracy, energies for the optimized geometries were recalculated using the solution-phase single-point calculations with a larger basis set, which is LANL2TZ(f) for V and 6-311 + G(d,p) for all other atoms. Solvation effects (solvent = toluene, ε = 2.374) are taken into account by performing single-point calculations with the SMD

model[77]. The final free energies reported in the article are the large basis set single-point energies corrected by gas-phase Gibbs free energy correction (at 298.15 K).

Data availability

All relevant data are available within the article as well as its Supplementary Information and from the corresponding authors on request. Crystallographic data for structures **3d**, **3p** and **3q** reported in this article have been deposited at the Cambridge Crystallographic Data Centre, under deposition numbers CCDC 2212869, 2212868 and 2212870, respectively. These data can be obtained free of charge from The Cambridge Crystallographic Data Centre via https://www.ccdc.cam.ac.uk/structures/.

References

1. Zhang, Z., Song, J. & Han, B. Catalytic transformation of lignocellulose into chemicals and fuel products in ionic liquids. *Chem. Rev.* **117**, 6834–6880 (2017).
2. Sun, Z., Fridrich, B., de Santi, A., Elangovan, S. & Barta, K. Bright side of lignin depolymerization: toward new platform chemicals. *Chem. Rev.* **118**, 614–678 (2018).
3. Zakzeski, J., Bruijnincx, P. C. A., Jongerius, A. L. & Weckhuysen, B. M. The catalytic valorization of lignin for the production of renewable chemicals. *Chem. Rev.* **110**, 3552–3599 (2010).
4. Wong, S. S., Shu, R., Zhang, J., Liu, H. & Yan, N. Downstream processing of lignin derived feedstock into end products. *Chem. Soc. Rev.* **49**, 5510–5560 (2020).
5. Li, C., Zhao, X., Wang, A., Huber, G. W. & Zhang, T. Catalytic transformation of lignin for the production of chemicals and fuels. *Chem. Rev.* **115**, 11559–11624 (2015).
6. Espro, C. et al. Sustainable production of pharmaceutical, nutraceutical and bioactive compounds from biomass and waste. *Chem. Soc. Rev.* **50**, 11191–11207 (2021).
7. Li, H., Bunrit, A., Li, N. & Wang, F. Heteroatom-participated lignin cleavage to functionalized aromatics. *Chem. Soc. Rev.* **49**, 3748–3763 (2020).
8. Pelckmans, M., Renders, T., Van de Vyver, S. & Sels, B. F. Bio-based amines through sustainable heterogeneous catalysis. *Green. Chem.* **19**, 5303–5331 (2017).
9. Chen, Z. et al. Formal direct cross-coupling of phenols with amines. *Angew. Chem. Int. Ed.* **54**, 14487–14491 (2015).
10. Qiu, Z., Lv, L., Li, J., Li, C.-C. & Li, C.-J. Direct conversion of phenols into primary anilines with hydrazine catalyzed by palladium. *Chem. Sci.* **10**, 4775–4781 (2019).
11. Chen, Z., Zeng, H., Gong, H., Wang, H. & Li, C.-J. Palladium-catalyzed reductive coupling of phenols with anilines and amines: efficient conversion of phenolic lignin model monomers and analogues to cyclohexylamines. *Chem. Sci.* **6**, 4174–4178 (2015).
12. Elangovan, S. et al. From wood to tetrahydro-2-benzazepines in three waste-free steps: modular synthesis of biologically active lignin-derived scaffolds. *ACS Cent. Sci.* **5**, 1707–1716 (2019).
13. Zhang, J., Liu, Y., Chiba, S. & Loh, T.-P. Chemical conversion of β-O-4 lignin linkage models through Cu-catalyzed aerobic amide bond formation. *Chem. Commun.* **49**, 11439–11441 (2013).
14. Blondiaux, E. et al. Bio-based aromatic amines from lignin-derived monomers. *ACS Sustainable Chem. Eng.* **7**, 6906–6916 (2019).
15. Li, H. et al. NH_2OH–mediated lignin conversion to isoxazole and nitrile. *ACS Sustainable Chem. Eng.* **6**, 3748–3753 (2018).
16. Liu, X. et al. Copper-catalyzed synthesis of benzanilides from lignin model substrates 2-phenoxyacetophenones under an air atmosphere. *New J. Chem.* **42**, 1223–1227 (2018).
17. Guo, T., Liu, T., He, J. & Zhang, Y. One-pot transformation of lignin and lignin model compounds into benzimidazoles. *Eur. J. Org. Chem.* **2022**, e202101152 (2022).
18. Cuypers, T. et al. Ni-Catalyzed reductive amination of phenols with ammonia or amines into cyclohexylamines. *Green. Chem.* **22**, 1884–1893 (2020).
19. Zheng, B. et al. Production of alkoxyl-functionalized cyclohexylamines from lignin-derived guaiacols. *Green. Chem.* **23**, 8441–8447 (2021).
20. Zhang, B. et al. Sustainable production of benzylamines from lignin. *Angew. Chem. Int. Ed.* **60**, 20666–20671 (2021).
21. Zhang, B. et al. Transition-metal-free synthesis of pyrimidines from lignin β-O-4 segments via a one-pot multi-component reaction. *Nat. Commun.* **13**, 3365 (2022).
22. Ding, Y. et al. Transition-metal-free synthesis of functionalized quinolines by direct conversion of β-O-4 model compounds. *Angew. Chem. Int. Ed.* **61**, e202206284 (2022).
23. Liu, J. et al. From alkylarenes to anilines via site-directed carbon-carbon amination. *Nat. Chem.* **11**, 71–77 (2019).
24. Liu, Y. et al. Successive cleavage and reconstruction of lignin β-O-4 models and polymer to access quinoxalines. *ChemSusChem* **15**, e202201401 (2022).
25. Rinesch, T. & Bolm, C. Cobalt-catalyzed oxidation of the β-O-4 bond in lignin and lignin model compounds. *ACS Omega* **3**, 8386–8392 (2018).
26. Zhang, C. et al. Cleavage of the lignin β-O-4 ether bond via a dehydroxylation–hydrogenation strategy over a NiMo sulfide catalyst. *Green. Chem.* **18**, 6545–6555 (2016).
27. Cai, X.-M. et al. BioAIEgens derived from rosin: how does molecular motion affect their photophysical processes in solid state? *Nat. Commun.* **12**, 1773 (2021).
28. Huang, S., Zhong, W., Zhang, X., Li, S. & Cai, X.-M. Research progress of photochemical-based aggregation-induced luminescent materials. *J. For. Eng.* **7**, 34–45 (2022).
29. Zhao, Z., Zhang, H., Lam, J. W. Y. & Tang, B. Z. Aggregation-Induced emission: new vistas at the aggregate level. *Angew. Chem. Int. Ed.* **59**, 9888–9907 (2020).
30. Li, X. et al. "Irregular" aggregation-induced emission luminogens. *Coord. Chem. Rev.* **418**, 213358 (2020).
31. Lee, M. M. S. et al. Leveraging bacterial survival mechanism for targeting and photodynamic inactivation of bacterial biofilms with red natural AIEgen. *Cell Rep. Phys. Sci.* **3**, 100803 (2022).
32. Ling, X. et al. Photoactivatable dihydroalkaloids for cancer cell imaging and chemotherapy with high spatiotemporal resolution. *Mater. Horiz.* **7**, 2696–2701 (2020).
33. Li, W., Chen, Z., Yu, H., Li, J. & Liu, S. Wood-derived carbon materials and light-emitting materials. *Adv. Mater.* **33**, 2000596 (2021).
34. Sun, L., Wang, X., Shi, J., Yang, S. & Xu, L. Kaempferol as an AIE-active natural product probe for selective Al^{3+} detection in Arabidopsis thaliana. *Spectrochim. Acta Part A: Mol. Biomol. Spectrosc.* **249**, 119303 (2021).
35. Long, R. et al. Novel natural myricetin with AIE and ESIPT characteristics for selective detection and imaging of superoxide anions in vitro and in vivo. *Chem. Commun.* **55**, 10912–10915 (2019).
36. Yan, L., Li, R., Shen, W. & Qi, Z. Multiple–color AIE coumarin–based schiff bases and potential application in yellow OLEDs. *J. Lumin.* **194**, 151–155 (2018).
37. Duan, L. et al. Slight substituent modification in coumarin molecular structures for strong solid emission and application in light-emitting devices. *Dyes Pigment* **174**, 108117 (2020).
38. Ma, Z. et al. Seeking brightness from nature: J-aggregation-induced emission in cellulolytic enzyme lignin nanoparticles. *ACS Sustainable Chem. Eng.* **6**, 3169–3175 (2018).
39. Shi, N. et al. Lignosulfonate/diblock copolymer polyion complexes with aggregation-enhanced and pH-switchable fluorescence for information storage and encryption. *Int. J. Biol. Macromol.* **187**, 722–731 (2021).

40. Xue, Y. et al. Aggregation-induced emission: the origin of lignin fluorescence. *Polym. Chem.* **7**, 3502–3508 (2016).
41. Mei, J. et al. Aggregation-induced emission: the whole is more brilliant than the parts. *Adv. Mater.* **26**, 5429–5479 (2014).
42. Liu, C. et al. Functionalization of silk by AIEgens through facile bioconjugation: full-color fluorescence and long-term bioimaging. *Angew. Chem. Int. Ed.* **60**, 12424–12430 (2021).
43. Chen, Y. et al. D–A type NIR-II organic molecules: strategies for the enhancement fluorescence brightness and applications in NIR-II fluorescence imaging-navigated photothermal therapy. *Adv. Healthc. Mater.* **11**, 2201158 (2022).
44. Etherington, M. K. et al. Regio- and conformational isomerization critical to design of efficient thermally-activated delayed fluorescence emitters. *Nat. Commun.* **8**, 14987 (2017).
45. Lei, Z. & Zhang, F. Molecular engineering of NIR-II fluorophores for improved biomedical detection. *Angew. Chem. Int. Ed.* **60**, 16294–16308 (2021).
46. Wu, T.-L. et al. Diboron compound-based organic light-emitting diodes with high efficiency and reduced efficiency roll-off. *Nat. Photonics* **12**, 235–240 (2018).
47. Gu, Y. et al. Chlorination-mediated π–π stacking enhances the photodynamic properties of a NIR-II emitting photosensitizer with extended conjugation. *Angew. Chem. Int. Ed.* **63**, e202303476 (2023).
48. Li, D. et al. Add the finishing touch: molecular engineering of conjugated small molecule for high-performance AIE luminogen in multimodal phototheranostics. *Small* **17**, 2102044 (2021).
49. Li, X. et al. Biodegradable π-conjugated oligomer nanoparticles with high photothermal conversion efficiency for cancer theranostics. *ACS Nano* **13**, 12901–12911 (2019).
50. Wan, X., Li, C., Zhang, M. & Chen, Y. Acceptor–donor–acceptor type molecules for high performance organic photovoltaics – chemistry and mechanism. *Chem. Soc. Rev.* **49**, 2828–2842 (2020).
51. Guo, T. et al. Copper-catalyzed three-component formal [3+1+2] benzannulation for carbazole and indole synthesis. *J. Org. Chem.* **85**, 9117–9128 (2020).
52. Uoyama, H., Goushi, K., Shizu, K., Nomura, H. & Adachi, C. Highly efficient organic light-emitting diodes from delayed fluorescence. *Nature* **492**, 234–238 (2012).
53. Zhang, D. et al. Efficient and stable deep-blue fluorescent organic light-emitting diodes employing a sensitizer with fast triplet upconversion. *Adv. Mater.* **32**, 1908355 (2020).
54. Liu, Z. et al. AIE-active luminogens as highly efficient free-radical ROS photogenerator for image-guided photodynamic therapy. *Chem. Sci.* **13**, 3599–3608 (2022).
55. Zhang, Q. et al. Design of efficient thermally activated delayed fluorescence materials for pure blue organic light emitting diodes. *J. Am. Chem. Soc.* **134**, 14706–14709 (2012).
56. Roy, J., Jana, A. K. & Mal, D. Recent trends in the synthesis of carbazoles: an update. *Tetrahedron* **68**, 6099–6121 (2012).
57. Schmidt, A. W., Reddy, K. R. & Knölker, H.-J. Occurrence, biogenesis, and synthesis of biologically active carbazole alkaloids. *Chem. Rev.* **112**, 3193–3328 (2012).
58. Banerjee, A., Kundu, S., Bhattacharyya, A., Sahu, S. & Maji, M. S. Benzannulation strategies for the synthesis of carbazoles, indolocarbazoles, benzocarbazoles, and carbolines. *Org. Chem. Front.* **8**, 2710–2771 (2021).
59. Banerjee, A., Guin, A., Saha, S., Mondal, A. & Maji, M. S. Formal [4 + 2] benzannulation of 2-alkenyl indoles with aldehydes: a route to structurally diverse carbazoles and bis-carbazoles. *Org. Biomol. Chem.* **17**, 1822–1826 (2019).
60. Saha, S., Banerjee, A. & Maji, M. S. Brønsted acid catalyzed one-pot benzannulation of 2-alkenylindoles under aerial oxidation: a route to carbazoles and indolo[2,3-a]carbazole alkaloids. *Org. Lett.* **20**, 6920–6924 (2018).
61. Banerjee, A. & Maji, M. S. A Brønsted acid catalyzed cascade reaction for the conversion of indoles to α-(3-Indolyl) ketones by using 2-benzyloxy aldehydes. *Chem. Eur. J.* **25**, 11521–11527 (2019).
62. Son, S. & Toste, F. D. Non-oxidative vanadium-catalyzed C-O bond cleavage: application to degradation of lignin model compounds. *Angew. Chem. Int. Ed.* **49**, 3791–3794 (2010).
63. Pinheiro, P. F. et al. Semisynthetic phenol derivatives obtained from natural phenols: antimicrobial activity and molecular properties. *J. Agric. Food Chem.* **66**, 323–330 (2018).
64. Shang, Y. et al. Pd-Catalyzed C–H olefination of (Hetero)arenes by using saturated ketones as an olefin source. *Angew. Chem. Int. Ed.* **52**, 1299–1303 (2013).
65. Yu, Y. et al. How do molecular interactions affect fluorescence behavior of AIEgens in solution and aggregate states? *Sci. China Chem.* **65**, 135–144 (2022).
66. Yuan, W. Z. et al. Efficient solid emitters with aggregation-induced emission and intramolecular charge transfer characteristics: molecular design, synthesis, photophysical behaviors, and OLED application. *Chem. Mater.* **24**, 1518–1528 (2012).
67. Pashazadeh, R. et al. An iminodibenzyl–quinoxaline–iminodibenzyl scaffold as a mechanochromic and dual emitter: donor and bridge effects on optical properties. *Chem. Commun.* **54**, 13857–13860 (2018).
68. Zuo, K. et al. Theoretical insight into the photodeactivation pathway of the tetradentate Pt(II) complex: the π-conjugation effect. *Appl. Organomet. Chem.* **32**, e4220 (2018).
69. Mei, J., Leung, N. L. C., Kwok, R. T. K., Lam, J. W. Y. & Tang, B. Z. +Aggregation-induced emission: together we shine, united we soar! *Chem. Rev.* **115**, 11718–11940 (2015).
70. Fang, M. M., Yang, J. & Li, Z. Light emission of organic luminogens: generation, mechanism and application. *Prog. Mater. Sci.* **125**, 100914–100982 (2022).
71. Lee, C., Yang, W. & Parr, R. G. Development of the colle-salvetti correlation-energy formula into a functional of the electron density. *Phys. Rev. B.* **37**, 785–789 (1988).
72. Becke, A. D. Density functional thermochemistry. III. The role of exact exchange. *J. Chem. Phys.* **98**, 5648–5652 (1993).
73. Grimme, S., Antony, J., Ehrlich, S. & Krieg, H. A consistent and accurate Ab initio parametrization of density functional dispersion correction (DFT-D) for the 94 elements H-Pu. *J. Chem. Phys.* **132**, 154104 (2010).
74. Frisch, M. J. et al. Gaussian 09, Revision E.01; Gaussian, Inc.: Wallingford, CT, 2013.
75. Fukui, K. Formulation of the reaction coordinate. *J. Phys. Chem.* **74**, 4161–4163 (1970).
76. Fukui, K. The path of chemical reactions - The IRC Approach. *Acc. Chem. Res.* **14**, 363–368 (1981).
77. Marenich, A. V., Cramer, C. J. & Truhlar, D. G. Universal solvation model based on solute electron density and on a continuum model of the solvent defined by the bulk dielectric constant and atomic surface tensions. *J. Phys. Chem. B.* **113**, 6378–6396 (2009).

Acknowledgements

Support from the National Natural Science Foundation of China (22078317, 22108272, 21601087, 22073066), Natural Science Foundation of Jiangsu Province (BK20231296), the science and technology bureau of Dalian city (No. 2021RT04) and Technical University of Munich.

Author contributions

T.Z., B.Z. and X.-M.C. conceived the study and directed the project; T.G. and B.Z. designed and performed the experiments; W.Z. and D.X. performed the control experiments; Y.L., X.Z. and X.-M.C. performed

photophysical investigation for AIEgens; D.P. and G.H. performed the DFT calculations. H.W. performed a part of HPLC measurements. B.Z., X.-M.C. and G.H. wrote the manuscript. F.E.K. and T.Z. improved the manuscript. All the authors discussed the results and commented on the manuscript.

Competing interests
The authors declare no competing interests.

Additional information
Supplementary information The online version contains supplementary material available at https://doi.org/10.1038/s41467-023-41681-0.

Correspondence and requests for materials should be addressed to Xu-Min Cai, Genping Huang, Bo Zhang or Tao Zhang.

Peer review information *Nature Communications* thanks the anonymous reviewers for their contribution to the peer review of this work. A peer review file is available.